

APPENDIX CONTENTS

- **Appendix A: Dataset Details** Page 15
- **Appendix B: Implementation Details** Page 16
- **Appendix C: Additional Experiments** Page 16
- **Appendix D: Details on Khatri-Rao Clustering and Matrix Decomposition** Page 19
- **Appendix E: Proofs** Page 22

Appendix A DATASET DETAILS

As stated in Section 9.1, in our experiments, we consider 13 synthetic and real-world datasets commonly used as benchmarks for clustering tasks. The datasets we consider reflect diverse data distributions, clustering structures and application domains. Next, we describe each dataset in detail.

- The MNIST dataset [15], available via PyTorch [19] or CLUSTPy [17], is a collection of 28×28 (vectorized) grayscale images of handwritten digits. We draw a stratified subsample of 25000 images, ensuring that the original class proportions across the ten digit clusters are preserved. We rescale all pixel values by dividing by the maximum.
- The DOUBLE MNIST dataset is derived from MNIST by horizontally concatenating pairs of digit images. Each sample is a 28×56 (vectorized) grayscale image obtained by placing one 28×28 digit in the left position and another in the right position, and the label encodes the ordered pair of digits, yielding 100 clusters in total. For our experiments, we generate 10000 such composite images using the procedure described above, resulting in an approximately uniform distribution over all digit pairs. Unlike the MNIST dataset, the DOUBLE MNIST dataset by construction admits a natural clustering with a Khatri-Rao structure. We rescale all pixel values by dividing by the maximum.
- The HAR dataset, available via the UCI REPOSITORY [12] or CLUSTPy [17], consists of sensor readings collected from smartphone accelerometers and gyroscopes during human activity monitoring. There are 10299 data points. Each data point is represented as a multivariate feature vector of dimension 561 derived from raw time-series measurements, and the dataset includes 6 activity clusters such as walking, standing and sitting. We standardize each feature by subtracting its mean and dividing by its standard deviation.
- The OLIVETTI FACES dataset, available via SCIKIT-LEARN [20] or CLUSTPy [17], contains (vectorized) grayscale facial images of 40 individuals, with 10 images per subject captured under varying lighting conditions, facial expressions, and poses. Each image has resolution 64×64 pixels. We standardize each feature by subtracting its mean and dividing by its standard deviation.
- The CMU FACES dataset, available via the UCI REPOSITORY [12] or CLUSTPy [17], contains grayscale facial images of 20 persons varying their pose (up, straight, left and right) and expression (neutral, happy, sad, angry), and shown with and without sunglasses. In total, there are 624 images. The

original images with a resolution of 30×32 pixels are vectorized and each feature is standardized by subtracting its mean and dividing by its standard deviation.

- The SYMBOLS dataset, available via CLUSTPy⁶ [17], consists of vectorized handwritten symbols. Each sample corresponds to a time series obtained from the drawing trajectory of a symbol. The symbols are drawn by 13 different individuals. The dataset contains a total of 1020 data points, each with 398 measurements. The data points are organized into 6 natural clusters. We standardize each feature by subtracting its mean and dividing by its standard deviation.
- The STICKFIGURES dataset [9], available via CLUSTPy [17], consists of 900 synthetic (vectorized) silhouette images of human stick figures generated under varying poses. Each image has a resolution of 20×20 pixels. Examples of such images are given in Figure 1. Each image is provided at a fixed resolution and captures a simplified body configuration defined by joint positions and limb orientations, resulting in 9 distinct pose-based clusters. We rescale all pixel values by dividing by the maximum.
- The OPTDIGITS dataset, available via the UCI REPOSITORY [12] or CLUSTPy [17], contains 5620 (vectorized) handwritten digit images represented as 8×8 grayscale pixel grids. We standardize each feature by subtracting its mean and dividing by its standard deviation.
- The CLASSIFICATION dataset, sourced by SCIKIT-LEARN [20], is a synthetic dataset. While it was originally designed for benchmarking classifiers, it is also useful for evaluating clustering algorithms which simply discard class labels until the evaluation of the clustering results. Each class for classification corresponds to a cluster. Except in the experiments where we vary the number of data points, features, or clusters, the dataset consists of 5000 samples organized into 100 clusters. The data are generated with 10 informative features, with no redundant or repeated features, ensuring that all dimensions contribute meaningfully to class separability. We standardize each feature by subtracting its mean and dividing by its standard deviation.
- The CHAMELEON dataset, available via the CLUSTBENCH Benchmark Suite [8], consists of 10000 two-dimensional point clouds exhibiting complex, nonconvex cluster shapes with varying densities [11]. The dataset corresponds to the configuration shown at the bottom of Figure 4, augmented with a substantial proportion of uniformly distributed data points that do not belong to any natural cluster.
- The SOYBEAN LARGE dataset, available via the UCI REPOSITORY [12] or CLUSTPy [17], is a dataset of categorical features. It consists of 562 plant samples belonging to one of 15 classes. For each plant, there are 35 observed categorical attributes describing the plant. After encoding categorical attributes numerically, we standardize each feature by subtracting its mean and dividing by its standard deviation.
- The BLOBS dataset, sourced by SCIKIT-LEARN [20], is a synthetic dataset specifically designed for controlled evaluation of clustering algorithms that consists of data points grouped

⁶The dataset is also available at: <https://www.timeseriesclassification.com/index.php>

1741 around isotropic Gaussian clusters. Each cluster has stan-
 1742 dard deviation 1. The dataset consists of 5000 2-dimensional
 1743 data points, arranged in 100 clusters, except in the experi-
 1744 ments where we vary the number of data points, features
 1745 and clusters. We standardize each feature by subtracting its
 1746 mean and dividing by its standard deviation.
 1747

- The R15 dataset, available via the CLUSTBENCH benchmark
 1748 suite [8], consists of 600 two-dimensional data points form-
 1749 ing 15 Gaussian clusters. The cluster centroids in R15 are
 1750 not arranged on a regular grid but exhibit non-uniform
 1751 inter-cluster distances. We standardize each feature by sub-
 1752 tracting its mean and dividing by its standard deviation.

Appendix B IMPLEMENTATION DETAILS

In this section, we discuss implementation details for all the algorithms considered in the experiments presented in Section 9.

Implementation details of the naïve approach to Khatri-Rao clustering. For the naïve Khatri-Rao clustering baseline used in our experiments, we first run the SCIKIT-LEARN [20] implementation of standard k -MEANS to extract the desired number of cluster centroids. For instance, if the goal is to extract two sets of h_1 and h_2 protocentroids, k -MEANS retrieves $h_1 h_2$ clusters. Then, using a coordinate-descent procedure implemented in Python with closed-form updates, we decompose a set of centroids into two smaller sets of protocentroids whose Khatri-Rao product approximates the original centroids. The coordinate-descent procedure alternates between updating the protocentroids of the first and second set, holding the other set fixed. At each step, we use the closed-form updates illustrated in Section 5 (Equation (8)). The procedure stops either when a maximum number of iterations is reached (5000 by default) or when the total sum of squared differences between the initial centroids and the Khatri-Rao aggregation of the protocentroids becomes smaller than a user-specified threshold (10^{-4} by default). Upon termination of the described coordinate-descent procedure, we have the output sets of protocentroids. The corresponding centroids are readily obtained by aggregating protocentroids. To conclude, we assign each data point to the closest centroid. The implementation is available online in our code repository⁷.

Implementation details of standard k -MEANS. We rely on the well-established SCIKIT-LEARN implementation of standard k -MEANS. The two k -MEANS baselines (namely k -MEANS with $h_1 + h_2$ centroids and $h_1 h_2$ centroids) are obtained by simply specifying the number of centroids $h_1 + h_2$ and $h_1 h_2$ as input. In the scalability experiments, instead, to ensure a fair comparison, we use an implementation of k -MEANS which mirrors the implementation of KHATRI-RAO- k -MEANS described next.

Implementation details of KHATRI-RAO- k -MEANS. Our experiments rely on a simple Python implementation of KHATRI-RAO- k -MEANS that is purely built on NUMPY⁸, taking advantage of vectorized operations for efficiency. Such implementation is available online⁹.

For initialization, by default we sample random data points as the initial protocentroids (as in Algorithm 1). Alternatively, we can

1799 adopt the strategy inspired by k -MEANS++ described in Section 6,
 1800 which selects representative data points based on squared-distance
 1801 criteria. Our implementation of this strategy either deterministically
 1802 chooses the data point farthest from the previously selected cen-
 1803 troids, or samples data points with probability proportional to their
 1804 distance from those centroids. After initialization, we iteratively
 1805 compute assignments, protocentroid and corresponding centroids.
 1806 Thanks to the closed-form updates introduced in Section 6, the
 1807 updates of protocentroids (and centroids) are implemented in a
 1808 fully-vectorized manner. At each iteration we monitor convergence
 1809 by tracking the movement of all reconstructed centroids; the algo-
 1810 rithm terminates once this movement falls below a user-specified
 1811 threshold or a maximum number of iterations is reached.

1812 During the execution of the algorithm, in case empty clusters
 1813 arise, they are handled by reinitializing the corresponding proto-
 1814 centroid to a random data point.

1815 Our implementation is deliberately simple and easy to follow. In
 1816 the future, more optimized or parallelized implementations could
 1817 be developed for larger-scale settings.

1818 KHATRI-RAO- k -MEANS admits both a time-efficient and a memory-
 1819 efficient implementation. Algorithm 1 presents the memory-efficient
 1820 implementation that avoids storing the full set of centroids by com-
 1821 puting them on the fly from the stored set of protocentroids. This
 1822 approach can reduce memory requirements, particularly when the
 1823 number of clusters is large since memory requirements only grow
 1824 additively with the total number of protocentroids instead of multi-
 1825 plicatively. For example, $h_1 h_2$ clusters demand storing only $h_1 + h_2$
 1826 protocentroids instead of $h_1 h_2$ centroids. However, computing
 1827 centroids on the fly incurs a runtime overhead. A time-efficient im-
 1828 plementation is obtained by computing centroids once and storing
 1829 them.

1830 **Implementation details of standard deep clustering algo-
 1831 rithms.** For DKM and IDEC, we rely on the off-the-shelf PyTorch-
 1832 based implementations provided by the CLUSTPy library¹⁰. To find
 1833 initial centroids, DKM and IDEC use the SCIKIT-LEARN imple-
 1834 mentation of standard k -MEANS.

1835 **Implementation details of Khatri-Rao deep clustering algo-
 1836 rithms.** For the implementation of Khatri-Rao deep clustering
 1837 algorithms, we build the implementation of KHATRI-RAO DKM and
 1838 KHATRI-RAO IDEC on top of the CLUSTPy implementations of the
 1839 corresponding standard deep clustering algorithms.

1840 Extending the CLUSTPy implementation of a standard deep clus-
 1841 tering algorithm to the Khatri-Rao clustering paradigm is straight-
 1842 forward. During initialization, we rely on our implementation of
 1843 KHATRI-RAO- k -MEANS to obtain initial protocentroids. We then re-
 1844 parameterize the centroids to satisfy the Khatri-Rao structure and
 1845 adjust the autoencoder parameters to conform to the Hadamard-
 1846 decomposition reparameterization. Our implementation of Khatri-
 1847 Rao deep clustering algorithms is available online¹¹.

Appendix C ADDITIONAL EXPERIMENTS

This section reports additional experimental results that comple-
 1849 ment the evaluation presented in Section 9. First, we empirically

⁷<https://github.com/maciap/KhatriRaoClustering/blob/main/scripts/KRkmeansExperimentsLib.py>

⁸<https://numpy.org>

⁹<https://github.com/maciap/KhatriRaoClustering/tree/main/KathriRaokMeans>

¹⁰<https://github.com/collinleiber/ClustPy>

¹¹<https://github.com/maciap/KhatriRaoClustering/tree/main/KhatriRaoDeepClustering>

1857 assess the scalability of KHATRI-RAO- k -MEANS by measuring runtime
 1858 and peak memory usage as the clustering tasks grow in size.
 1859 Second, we study the effect of the number of centroids on the
 1860 clustering performance of KHATRI-RAO- k -MEANS and the corre-
 1861 sponding baselines. Finally, we turn to deep clustering and evaluate
 1862 how compressing the autoencoder via the Hadamard decomposi-
 1863 tion affects clustering performance and training stability. Unless
 1864 specified otherwise, all experimental settings are the same as for
 1865 the experiments presented in Section 9.

1866 **Scalability.** The goal of Khatri-Rao clustering is to extract accurate
 1867 data summaries that are more succinct than those extracted by
 1868 standard clustering methods. Our experiments show that Khatri-
 1869 Rao clustering can yield more succinct clustering-based summaries
 1870 while maintaining comparable accuracy. However, it is also impor-
 1871 tant to ensure that the advantages provided by Khatri-Rao cluster-
 1872 ing are not undermined by significantly worse scalability. Section 6
 1873 discusses the theoretical asymptotic time and space complexity of
 1874 KHATRI-RAO- k -MEANS. According to the discussion, KHATRI-RAO-
 1875 k -MEANS has the same asymptotic time complexity as k -MEANS. In
 1876 addition, KHATRI-RAO- k -MEANS can reduce the memory usage of
 1877 k -MEANS when the number of clusters and hence centroids to be
 1878 represented grows. To complement the analysis of time and space
 1879 complexity, we conduct an empirical scalability analysis.

1880 The results of the empirical scalability analysis are summarized
 1881 in Figures 10 and 11. The figures show runtime (in seconds) for
 1882 a single execution of an algorithm and peak memory usage (in
 1883 Mebibytes) as the number of data points, features and centroids
 1884 increase for the BLOBS and CLASSIFICATION datasets. In particular,
 1885 we vary the number of data points in {4000, 8000, 12000, 16000} with
 1886 100 clusters and 100 features, we vary the number of features in
 1887 {10000, 15000, 20000, 25000} with 1000 data points and 100 clusters,
 1888 and we vary the number of clusters in {2500, 5000, 7500, 10000}
 1889 with 20000 data points and 100 features.

1890 The results suggest that KHATRI-RAO- k -MEANS clustering in-
 1891 troduces a runtime overhead compared to standard k -MEANS, but
 1892 this overhead does not significantly increase as the problem size
 1893 increases. Instead, the overhead remains nearly constant as the
 1894 number of data points, features and centroids increase, in line with
 1895 the time-complexity discussion in Section 6.

1896 The two-phase naïve approach to Khatri-Rao k -Means is usu-
 1897 ally the slowest algorithm, except when the number of centroids
 1898 becomes large and KHATRI-RAO- k -MEANS can become slower than
 1899 the naïve approach to Khatri-Rao k -Means. On the other hand,
 1900 standard k -MEANS is consistently the fastest algorithm.

1901 As for memory requirements, KHATRI-RAO- k -MEANS often in-
 1902 curs similar memory requirements as standard k -MEANS that uses
 1903 $h_1 + h_2$ vectors to represent centroids. On the other hand, k -MEANS
 1904 with $h_1 h_2$ centroids can be more memory demanding, particularly
 1905 when the number of centroids grows. Specifically, as the number of
 1906 centroids increases, k -MEANS with $h_1 h_2$ centroids uses up to about
 1907 2.7 times as much memory as KHATRI-RAO- k -MEANS in both the
 1908 BLOBS and CLASSIFICATION datasets. Furthermore, the gap grows
 1909 with the number of centroids, corroborating the space-complexity
 1910 discussion in Section 6.

1911 It is also of interest to investigate the scalability of KHATRI-RAO-
 1912 k -MEANS as a function of the number of protocentroids sets. For
 1913 the same experimental settings as in Figure 7, Figure 12 reports

1915 the runtime and memory usage of KHATRI-RAO- k -MEANS as the
 1916 number p of protocentroids sets varies in {2, 3, 4}, while keeping
 1917 a budget of 12 vectors to represent the centroids. As suggested by
 1918 the results, increasing the number of protocentroids leads to higher
 1919 runtime, as more centroids are computed. Memory usage may also
 1920 increase slightly, with variations always bounded by 5 mebibytes.
 1921 For reference, we additionally report the runtime and peak memory
 1922 usage of all baseline methods with $h_1 = h_2$. These measurements
 1923 are obtained on the original BLOBS and CLASSIFICATION datasets,
 1924 corresponding to relatively small problem instances.

1925 **Impact of the number of centroids.** To complement the pre-
 1926 liminary experiments presented in Section 9, Figure 13 shows the
 1927 inertia incurred by the KHATRI-RAO- k -MEANS and the baselines
 1928 under comparison as the number of ground-truth clusters k in the
 1929 data is varied within {25, 100, 225, 400, 625} in the BLOBS and CLAS-
 1930 SIFICATION datasets. The figure demonstrates that KHATRI-RAO- k -
 1931 MEANS consistently achieves significantly lower inertia than the
 1932 baselines at parity parameters (i.e., number of vectors to repre-
 1933 sent centroids). Standard k -MEANS with $h_1 h_2$ vectors to represent
 1934 centroids achieves the lowest inertia, although its advantage over
 1935 KHATRI-RAO- k -MEANS, which uses only $h_1 + h_2$ vectors, remains
 1936 consistently small.

1937 Finally, the naïve approach always incurs the highest inertia,
 1938 and its performance tends to worsen with the number of clusters,
 1939 which is not the case for the other algorithms under comparison.

1940 **Impact of the reparameterization on the autoencoder.** As
 1941 explained in Section 4.3, in Khatri-Rao deep clustering, we com-
 1942 press the autoencoder by reparameterizing its weights as Hadamard
 1943 product of low-rank factors.

1944 This reparameterization can impact training stability and cluster-
 1945 ing performance. Thus, in the following, we empirically investigate
 1946 the training stability and clustering performance as a function of
 1947 the rank of both Hadamard factors. In particular, the rank of the
 1948 Hadamard factors is varied in {20, 30, 40, 50, 60}.

1949 Figure 14 displays the value of the clustering quality metrics
 1950 monitored in this work for the BLOBS and CLASSIFICATION datasets
 1951 against the rank of each of two Hadamard factors. As the figure
 1952 suggests, the chosen rank can have an impact on the clustering
 1953 performance of Khatri-Rao deep clustering. However, such impact
 1954 is limited. Increasing the rank of both Hadamard factors from 10
 1955 to 60 results in changes of at most 0.1 across all metrics, with
 1956 most variations remaining below 0.05. On the BLOBS dataset, the
 1957 smallest rank considered (20) yields better clustering performance
 1958 than higher ranks. In this case, the implicit regularization induced
 1959 by the reparameterization as Hadamard product of low-rank factors
 1960 may be beneficial for clustering.

1961 For the BLOBS and CLASSIFICATION datasets, Figure 15 depicts
 1962 the evolution of the training loss over 500 epochs for both the un-
 1963 compressed autoencoder and the compressed autoencoder in case
 1964 the rank of both Hadamard factors is 20, 40 and 60. Although, par-
 1965 ticularly for the lower ranks, the compressed autoencoder exhibits
 1966 a slightly slower initial decrease in training loss compared to the
 1967 uncompressed autoencoder, it quickly converges to a comparable
 1968 loss level. Overall, the training loss decays smoothly and consis-
 1969 tently over iterations for both the uncompressed and compressed
 1970 autoencoders across all considered ranks.

1971
 1972

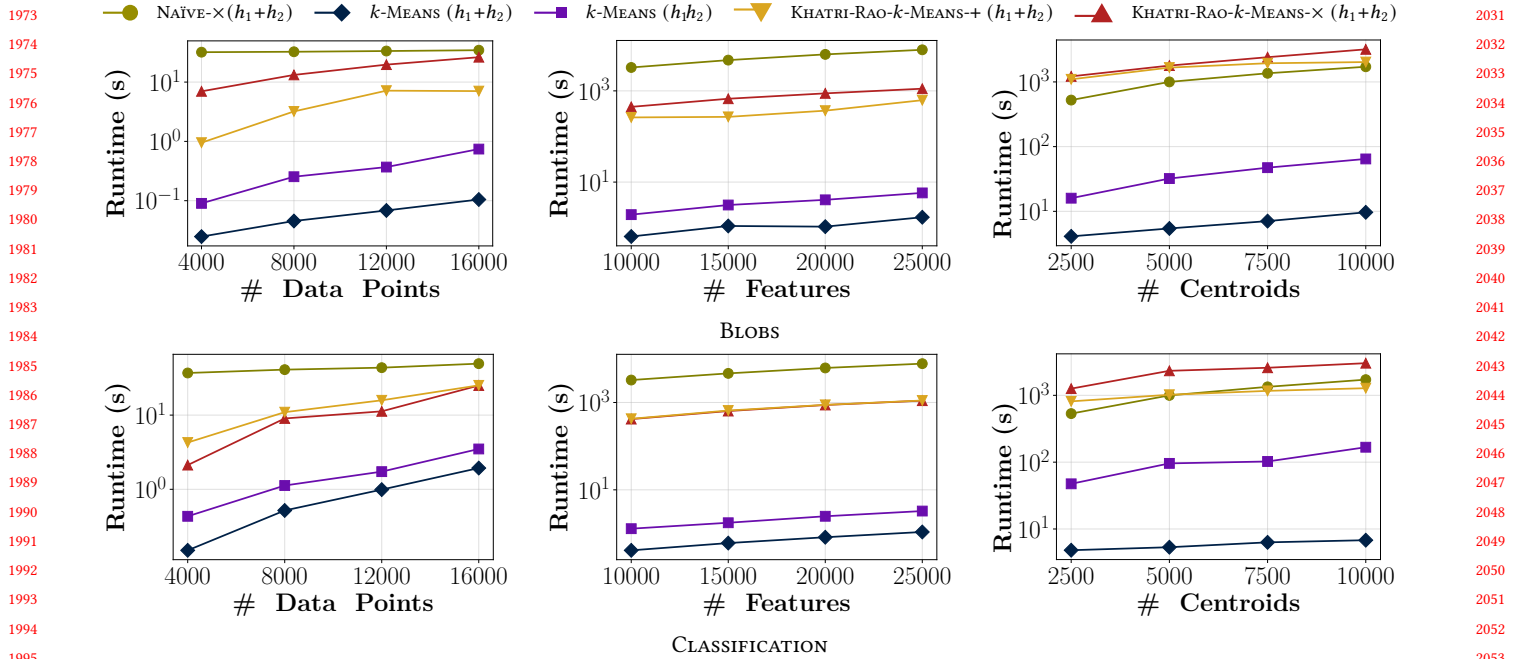


Figure 10: Experiments on BLOBS and CLASSIFICATION datasets. Runtime (in seconds) by number of data points n , number of features m and number of centroids k . Here, k-MEANS (h_1h_2) uses h_1h_2 vectors to represent centroids, while all other algorithms $h_1 + h_2$. The y-axis is on The y-axis is on a logarithmic scale.

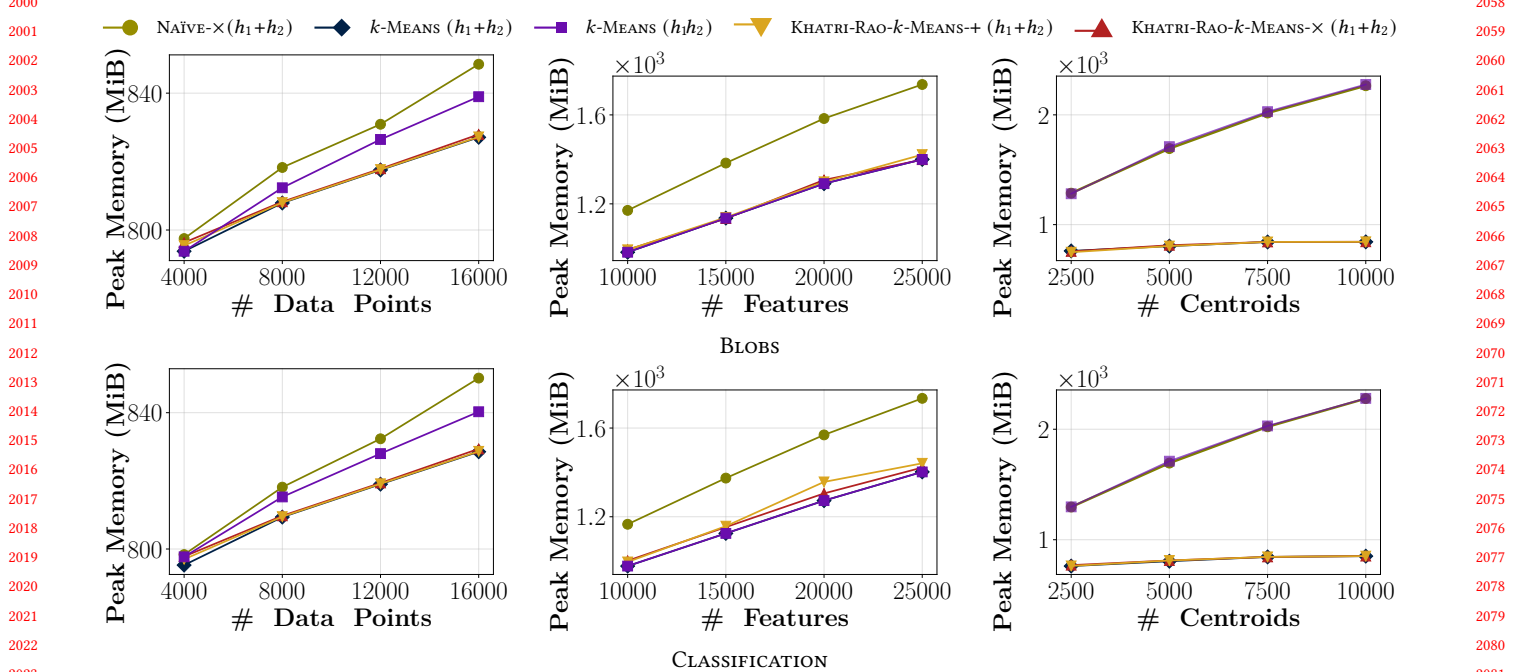


Figure 11: Experiments on BLOBS and CLASSIFICATION datasets. Peak memory usage (in Mebibytes) by number of data points n , number of features m and number of centroids k . Here, k-MEANS (h_1h_2) uses h_1h_2 vectors to represent centroids, while all other algorithms $h_1 + h_2$. The y-axis is on a logarithmic scale.

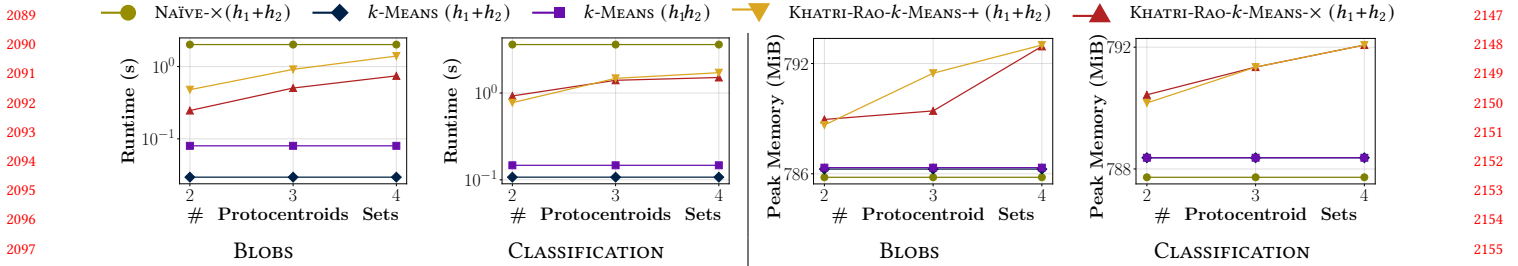


Figure 12: Experiments on BLOBS and CLASSIFICATION datasets. Runtime in seconds (left) and memory usage in Mebibytes (right) by number of sets of protocentroids. Here, KHATRI-RAO- k -MEANS always uses 12 total vectors to represent centroids. All baselines assume $h_1 = h_2 = 6$. The y-axis is on a logarithmic scale.

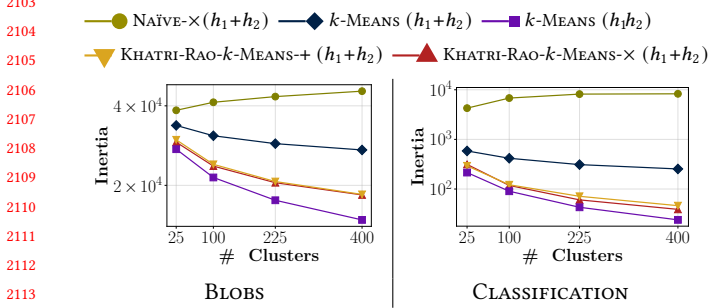


Figure 13: Experiments on BLOBS and CLASSIFICATION datasets. Inertia as a function of the number of ground-truth clusters k . Here, k-MEANS (h_1h_2) uses h_1h_2 vectors to represent centroids, while all other algorithms $h_1 + h_2$. The y-axis is on a logarithmic scale.

Appendix D DETAILS ON KHATRI-RAO CLUSTERING AND MATRIX DECOMPOSITION

As anticipated in Section 2, clustering is closely related to matrix decomposition. Both centroid-based clustering and matrix decomposition pursue the objective of summarizing data through a succinct set of prototypes. Many clustering problems such as k -Means can be seen as a particular case of matrix decomposition where one of the factor matrices is constrained to indicate cluster membership. In fact, it has been shown that the continuous relaxation of the k -Means cluster-membership indicators is given by the principal components of the data [7], establishing a direct link between k -Means clustering and principal component analysis, a prominent matrix-decomposition technique. Clustering via matrix decomposition has been successfully applied in different domains like text mining [22], graph mining [1, 13] and bioinformatics [2].

The established relationship between clustering and matrix factorization also extends to tensor data. Tensor decompositions can be used for clustering tensor data [14], with successful applications in areas like text mining across multiple languages [4], multilayer graph mining [3] and bioinformatics [21].

Given the close interplay between matrix (or tensor) decomposition and clustering, a natural question is how Khatri-Rao clustering fits within the broader framework of matrix decomposition.

In this section, we first review how standard k -Means clustering can be formulated as a constrained matrix-decomposition problem. Second, we show that also Khatri-Rao k -Means can be interpreted as a constrained instance of matrix decomposition. Then, we discuss the well-known example of nonnegative matrix factorization [18]. Finally, we present a simple illustrative experiment which anticipates the potential advantages of Khatri-Rao clustering in clustering via matrix decomposition.

k -Means clustering as matrix decomposition. The k -Means clustering problem can be formulated as approximating a data matrix by a product of lower-rank factors: one factor encodes cluster centroids and the other encodes cluster-membership assignments.

More specifically, the k -Means problem admits a natural reformulation as a constrained matrix decomposition task as follows. Let $\mathcal{D} = \{\mathbf{x}_1, \dots, \mathbf{x}_n\} \subset \mathbb{R}^m$ be the dataset and denote by $\Theta = \{\boldsymbol{\mu}_i\}_{i=1}^k$ the set of centroids, where $\boldsymbol{\mu}_i$ is the centroid of C_i . Introduce the assignment matrix $\mathbf{Z} \in \{0, 1\}^{n \times k}$, where $Z_{ji} = 1$ if $\mathbf{x}_j \in C_i$ and 0 otherwise, so that each data point is assigned to exactly one cluster (i.e., $Z_{1:k} = \mathbf{1}_n$). Let $\mathbf{C} \in \mathbb{R}^{k \times m}$ be the centroid matrix whose i -th row equals $\boldsymbol{\mu}_i^\top$. Collecting the data points in \mathcal{D} as the rows of a data matrix $\mathbf{D} \in \mathbb{R}^{n \times m}$, the inertia objective in Equation (1), minimized in k -Means, can be written compactly as:

$$Q_C(\mathcal{D}, \Theta) = \|\mathbf{D} - \mathbf{Z}\mathbf{C}\|_F^2 \quad (9)$$

under the aforementioned assignment constraints encoded in \mathbf{Z} . Here, $\|\mathbf{X}\|_F$ denotes the Frobenius norm of \mathbf{X} . Thus, the k -Means problem is equivalent to seeking a decomposition $\mathbf{D} \approx \mathbf{Z}\mathbf{C}$ under the constraint that \mathbf{Z} is a binary assignment matrix with one nonzero entry per row.

Khatri-Rao k -Means clustering as constrained matrix decomposition. Like standard k -Means clustering, Khatri-Rao k -Means clustering also admits a formulation in terms of matrix decomposition. To derive the formulation of Khatri-Rao k -Means as matrix decomposition, let us introduce matrices \mathbf{Z}_i and \mathbf{P}_i with $i = 1 \dots p$. Similarly to \mathbf{Z} for standard k -Means, matrices \mathbf{Z}_i have one-hot assignment vectors as rows. Matrix \mathbf{Z}_i assigns each data point to one of h_i protocentroids stored as rows of matrix \mathbf{P}_i . Then, the Khatri-Rao k -Means problem amounts to the minimization of:

$$Q_C(\mathcal{D}, \Theta) = \|\mathbf{D} - (\mathbf{Z}_1\mathbf{P}_1) \oplus (\mathbf{Z}_2\mathbf{P}_2) \dots \oplus (\mathbf{Z}_p\mathbf{P}_p)\|_F^2. \quad (10)$$

under the assignment constraints in matrices \mathbf{Z}_i . Hence, Khatri-Rao k -Means clustering induces a decomposition of the form $\mathbf{D} \approx$

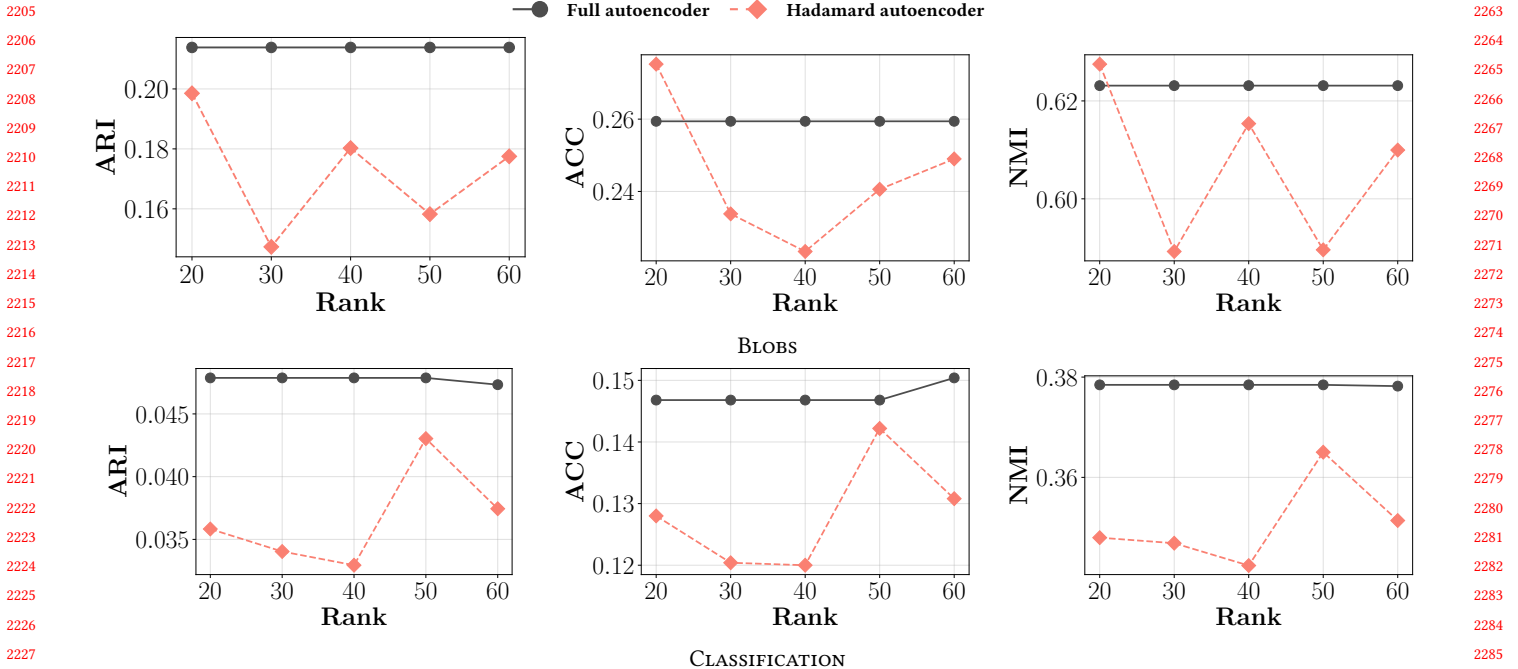


Figure 14: Experiments on BLOBS and CLASSIFICATION datasets. Unsupervised clustering accuracy (ACC), adjusted Rand index (ARI) and normalized mutual information (NMI) for KHATRI-RAO DKM against rank of both factors in the reparameterization of the autoencoder weights as Hadamard product of two low-rank factors.

$(Z_1 P_1) \oplus (Z_2 P_2) \dots \oplus (Z_p P_p)$ under the constraint that Z_i are binary assignment matrices with one nonzero entry per row. Such decomposition is illustrated in Figure 16.

Khatri-Rao clustering and the Hadamard decomposition. Equation (10) highlights the connection between Khatri-Rao k-Means and the Hadamard decomposition, studied in our previous work [6]. In the Hadamard decomposition, as in general matrix decomposition, the factors Z_i are unconstrained. As a result, summation does not introduce additional structure: the sum of q rank- r factors can represent matrices of rank at most qr , and summing two decompositions each using h vectors per factor is, in principle, equivalent to a single decomposition with $2h$ vectors per factor. In the setting of matrix decomposition, summation of multiple matrix decompositions merely reallocates expressiveness. By contrast, the Hadamard product can yield a more expressive model since the product of q rank- r factors can represent matrices of rank up to r^q , which explains the improved compression rates observed for the Hadamard decomposition in previous work [6, 10]. This expressiveness advantage is also the reason why we adopt the Hadamard product in the reparameterization of the autoencoder for Khatri-Rao deep clustering.

The expressiveness advantage of the Hadamard product over the sum in matrix decomposition, however, does not carry over to Khatri-Rao clustering. Once the factors Z_i are constrained to be one-hot cluster indicators, multiple decompositions combined additively are no longer equivalent in principle to a single enlarged factor. The discrete assignment structure prevents expressiveness

from being freely reallocated, so that summation can introduce genuinely new expressiveness.

The example of nonnegative matrix factorization. Nonnegative matrix factorization (NMF) exemplifies how clustering and matrix decomposition are fundamentally intertwined.

Given an integer k , NMF represents data as a product of nonnegative factors [16], imposing the model $D = WH$ with $W_{i,j} \geq 0 \forall i = 1 \dots n, j = 1 \dots k$ and $H_{i,j} \geq 0 \forall i = 1 \dots k, j = 1 \dots m$. NMF has emerged as a powerful approach to clustering, as its representations naturally induce groupings of data points and features.

It is known that optimizing NMF under the orthogonality constraint $W^T W = I$, i.e., solving:

$$\min_{W, H; W_{i,j} \geq 0 \forall i, j, H_{i,j} \geq 0 \forall i, j, W^T W = I} \|D - WH\|_F^2 \quad (11)$$

is equivalent to the k -MEANS problem (assuming positive data) [18].

As in the case of standard clustering, a Khatri-Rao variant of NMF asks to solve:

$$\begin{aligned} \min_{W_t, H_t} & \|D - (W_1 H_1) \oplus (W_2 H_2) \\ & \dots \oplus (W_p H_p)\|_F^2. \end{aligned} \quad (12)$$

Algorithms that solve the optimization problem in Equation (11) have been proposed in the literature [5]. Studying their extension to

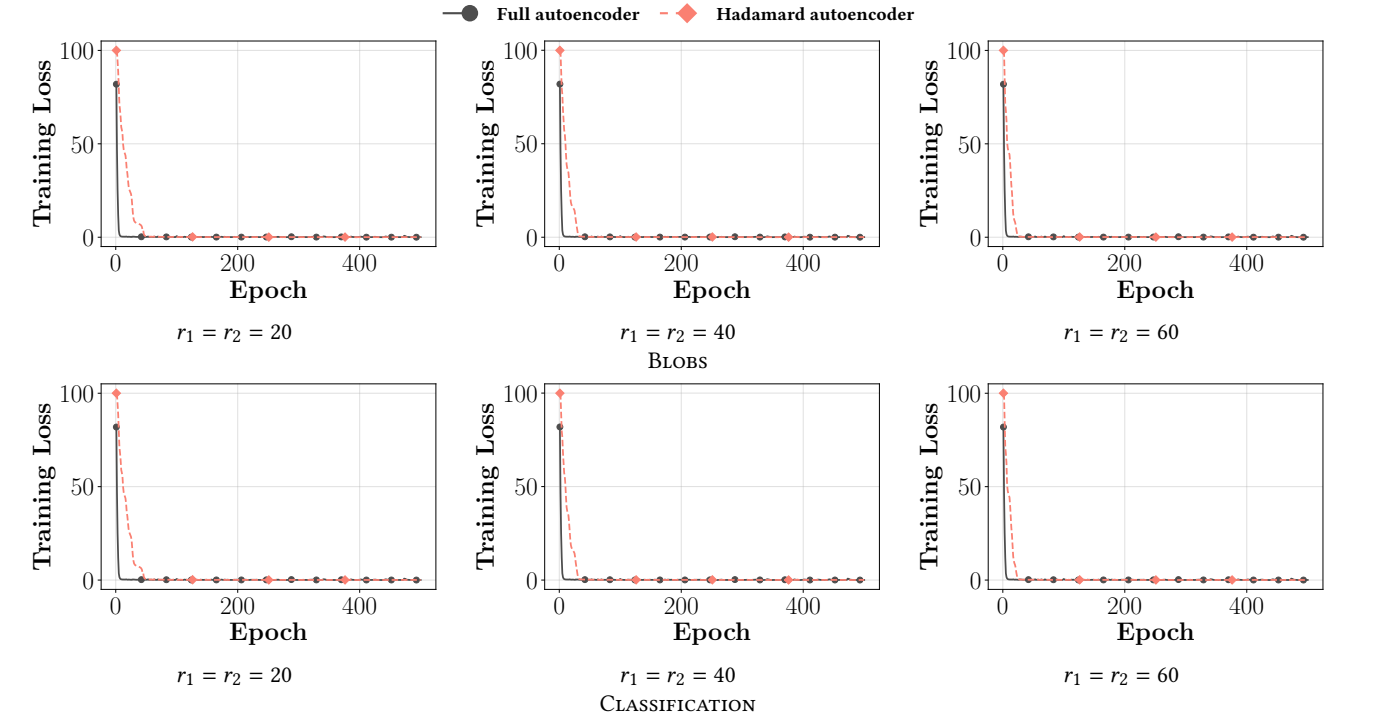


Figure 15: Experiments on BLOBS and CLASSIFICATION datasets. Training loss decay across 500 epochs for the unconstrained autoencoder and the autoencoder with weights reparameterized as the Hadamard product of two low-rank factors with ranks r_1 and r_2 . We set $r_1 = r_2$, and we show results for three different choices of r_1 and r_2 (20, 40 and 60).

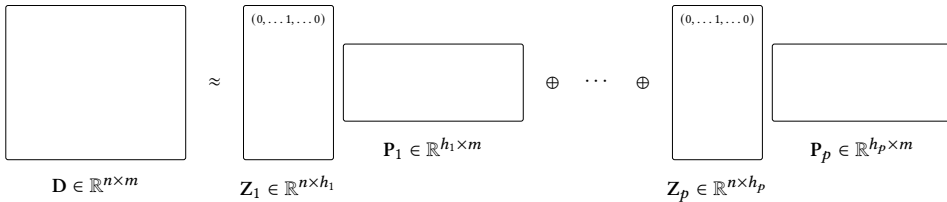


Figure 16: Diagram representing Khatri-Rao k -Means as matrix decomposition.

the Khatri-Rao clustering paradigm by addressing the optimization problem in Equation (12) is an exciting direction of future work.

D.1 Illustrative experiments.

To conclude, we carry out an illustrative experiment to anticipate empirically the benefits that Khatri-Rao clustering can provide to centroid-based clustering via matrix decomposition. This experiment is not intended to introduce a new state-of-the-art clustering method based on matrix decomposition, but to demonstrate the practical advantages that the Khatri-Rao clustering paradigm can potentially offer in this context through a simple approach. We focus on the case of two sets of protocentroids. Equations (9) and (10) express the k -Means and Khatri-Rao k -Means problems in terms of matrix decomposition, respectively. In this illustrative experiment, we address such problems via gradient-based optimization, relying on PyTorch for automatic differentiation. In particular, for

k -Means clustering, we define the model $D = ZC$, and we learn its parameters by optimizing the following loss function:

$$\sum_{i=1}^n \sum_{j=1}^k Z_{i,j} \|D_i - C_j\|^2. \quad (13)$$

Similarly, for Khatri-Rao clustering, we define the model $D = (Z_1 P_1) \oplus (Z_2 P_2)$, and we learn its parameters by optimizing the loss function in Equation (13) adapted to enforce the Khatri-Rao structure. For optimization purposes, we relax the constraints that matrices Z in standard clustering and Z_i in Khatri-Rao clustering are binary assignment matrices. Instead, each row encodes continuous soft assignments to all clusters. We run the optimization for 5000 epochs using the Adam optimizer, with gradients computed over the entire dataset at each epoch. To obtain one-hot assignment vectors, we first initialize the continuous soft assignments at random, and we apply the softmax function to ensure that assignments for each

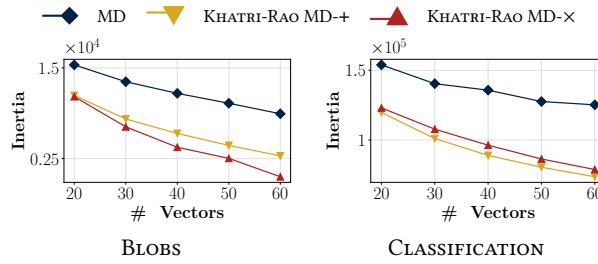


Figure 17: Experiments on BLOBS and CLASSIFICATION datasets. Inertia by number of vectors used to represent centroids for a simple approach to standard clustering via matrix decomposition (MD) and its Khatri-Rao variant with sum aggregator (KHATRI-RAO MD-+) and product aggregator (KHATRI-RAO MD-x). The y-axis is on a logarithmic scale.

data point sum to 1. During the optimization, the temperature of the softmax function is linearly annealed from 1 to 0.1 to progressively sharpen the assignments until they approach one-hot vectors. The learning rate is also annealed at the same time from 10^{-1} to 5×10^{-3} . More specifically, both temperature and learning rate follow linear schedules of the form $(1 - a_t)l_{start} + a_t l_{end}$, where l_{start} and l_{end} are either the initial and final temperature or learning rate and a_t increases linearly over epochs. To improve performance, we initialize the centroids (stored as rows of matrix C for standard clustering and as combinations of rows of matrices P_i for Khatri-Rao clustering) uniformly in the range of the data.

Upon termination of the 5000 epochs, we compute the hard inertia of the solution clustering by assigning each data point to the cluster with the highest assignment score. Because of the temperature annealing, highest assignment scores are typically close to 1 while the others approach 0.

The results of the described experiment for the BLOBS and CLASSIFICATION datasets are displayed in Figure 17. Here, we compare clustering via standard matrix decomposition (MD) and its Khatri-Rao clustering extension with sum aggregator (KHATRI-RAO MD-+) and product aggregator (KHATRI-RAO MD-x), as the number of vectors used to represent centroids varies in $\{20, 30, 40, 50, 60\}$. The results of the experiment indicate that the matrix decomposition approach to standard clustering incurs higher inertia than its Khatri-Rao counterpart. More specifically, standard matrix decomposition exhibits an inertia that is at least 83% and 28% higher than that achieved by any Khatri-Rao variant in the BLOBS and CLASSIFICATION datasets, respectively. The advantages provided by the Khatri-Rao clustering paradigm also tend to increase with the number of vectors used to represent centroids.

Appendix E PROOFS

In this section, we collect the proofs of the propositions stated in the paper.

Proof of Proposition 6.1.

PROOF. We illustrate the proof for the product aggregator. Consider the j -th protocentroid in the first set of protocentroids. The

optimal update for this protocentroid satisfies:

$$\theta_1^j = \arg \min_{\theta} \sum_{l=1}^{h_2} \sum_{x \in C_{j,l}} (x - \theta \odot \theta_2^l)^2.$$

Therefore θ_1^j can be found by computing the gradient of this sum of squared differences with respect to θ and equating it to the zero vector $\mathbf{0}$. Doing so, one obtains:

$$-2 \sum_{l=1}^{h_2} \sum_{x \in C_{j,l}} (x - \theta \odot \theta_2^l) \theta_2^l = \mathbf{0},$$

which holds if and only if:

$$\theta_1^j = \frac{\sum_{l=1}^{h_2} \sum_{x \in C_{j,l}} x \odot \theta_2^l}{\sum_{l=1}^{h_2} |C_{j,l}| \theta_2^l \odot \theta_2^l}.$$

The derivations for the second set of protocentroids are symmetric, and the proof for the sum aggregator is also similar. \square

Proof of Proposition 8.1.

PROOF. Assuming p protocentroid sets of equal size and exact budget usage, each set contains $h = \frac{b}{p}$ protocentroids, so the total number of centroids that can be represented is:

$$\left(\frac{b}{p}\right)^p.$$

Maximizing this function over $p > 0$ is equivalent to maximizing its logarithm:

$$p \log\left(\frac{b}{p}\right) = p \log b - p \log p,$$

where \log denotes the natural logarithm. Differentiating with respect to p yields:

$$\log\left(\frac{b}{p}\right) - 1,$$

which is positive for $p < \frac{b}{e}$ and negative for $p > \frac{b}{e}$. Moreover, the second derivative:

$$-\frac{1}{p} < 0 \quad (p > 0)$$

shows that the log-objective is strictly concave, and therefore attains a unique maximum at $p = \frac{b}{e}$ in the continuous domain.

When restricting to the divisor-only setting, the optimal value of p , p^{\max} , is required to be an integer that exactly divides b , so that $h^{\max} = \frac{b}{p^{\max}}$ is an integer. Since the objective is strictly increasing for $p < \frac{b}{e}$ and strictly decreasing for $p > \frac{b}{e}$, among all such admissible values the maximum is attained at one of the two values of p that are immediately below or above $\frac{b}{e}$ (when each exists). All other admissible divisors are necessarily further away from $\frac{b}{e}$, and therefore yield a strictly smaller objective value. \square

Proof of Proposition 8.2.

PROOF. We present the proof for the product aggregator. However, extension to different aggregator functions is straightforward.

First, to see why it must be $p^* \geq \log_{h_{\min}} k$, notice that, if $p^* < \log_{h_{\min}} k$ then $h_{\min}^{p^*} < k$, and $h_{\min}^{p^*}$ is the maximum number of centroids that can be represented using p^* sets of at least h_{\min}

2553 protocentroids. As regards the other inequality, to prove that $p^* \leq$
 2554 $\lceil \frac{k}{h_{\min}-1} \rceil$, it is sufficient to construct an example where all sets have
 2555 a protocentroid with all entries equal to 1 and the remaining at least
 2556 $h_{\min}-1$ protocentroids that are equal to centroids. Different sets
 2557 contain different centroids. In the illustrated scenario, each set of
 2558 protocentroids represents exactly at least $h_{\min}-1$ centroids. Thus,
 2559 $\lceil \frac{k}{h_{\min}-1} \rceil$ sets of protocentroids can always represent k centroids.
 2560 \square

2562 REFERENCES

- [1] Kamal Berahmand, Mehrnoush Mohammadi, Razieh Sheikhpour, Yuefeng Li, and Yue Xu. 2024. WSNMF: Weighted Symmetric Nonnegative Matrix Factorization for attributed graph clustering. *Neurocomputing* 566 (2024), 127041.
- [2] Jean-Philippe Brunet, Pablo Tamayo, Todd R Golub, and Jill P Mesirov. 2004. Metagenes and molecular pattern discovery using matrix factorization. *Proceedings of the national academy of sciences* 101, 12 (2004), 4164–4169.
- [3] Zitai Chen, Chuan Chen, Zibin Zheng, and Yi Zhu. 2019. Tensor Decomposition for Multilayer Networks Clustering. In *AAAI*. AAAI Press, 3371–3378.
- [4] Peter A. Chew, Brett W. Bader, Tamara G. Kolda, and Ahmed Abdellali. 2007. Cross-language information retrieval using PARAFAC2. In *KDD*. ACM, 143–152.
- [5] Seungjin Choi. 2008. Algorithms for orthogonal nonnegative matrix factorization. In *2008 ieee international joint conference on neural networks (ieee world congress on computational intelligence)*. IEEE, 1828–1832.
- [6] Martino Ciaperoni, Aristides Gionis, and Heikki Mannila. 2024. The Hadamard decomposition problem. *Data Mining and Knowledge Discovery* (2024), 1–42.
- [7] Chris Ding and Xiaofeng He. 2004. K-means clustering via principal component analysis. In *Proceedings of the twenty-first international conference on Machine learning*. 29.
- [8] Marek Gagolewski. 2022. A framework for benchmarking clustering algorithms. *SoftwareX* 20 (2022), 101270.
- [9] Stephan Günnemann, Ines Färber, Matthias Sebastian Rüdiger, and Thomas Seidl. 2014. SMVC: semi-supervised multi-view clustering in subspace projections. In *The 20th ACM SIGKDD International Conference on Knowledge Discovery and Data Mining*. ACM, 123–131.
- [10] Nam Hyeon-Woo, Moon Ye-Bin, and Tae-Hyun Oh. 2021. FedPara: Low-rank Hadamard Product for Communication-Efficient Federated Learning. In *International Conference on Learning Representations*.
- [11] George Karypis, Eui-Hong Han, and Vipin Kumar. 1999. Chameleon: Hierarchical Clustering Using Dynamic Modeling. *Computer* 32, 8 (1999), 68–75. <https://doi.org/10.1109/2.781637>
- [12] Markelle Kelly, Rachel Longjohn, and Kolby Nottingham. 2023. The UCI machine learning repository.
- [13] Mikhail Khodak, Neil A. Tenenholz, Lester Mackey, and Nicolò Fusi. 2021. Initialization and Regularization of Factorized Neural Layers. In *ICLR*. OpenReview.net.
- [14] Tamara G. Kolda and Brett W. Bader. 2009. Tensor Decompositions and Applications. *SIAM Rev* 51, 3 (2009), 455–500.
- [15] Yann LeCun, Léon Bottou, Yoshua Bengio, and Patrick Haffner. 1998. Gradient-based learning applied to document recognition. *Proc. IEEE* 86, 11 (1998), 2278–2324.
- [16] Daniel Lee and H Sebastian Seung. 2000. Algorithms for non-negative matrix factorization. *Advances in neural information processing systems* 13 (2000).
- [17] Collin Leiber, Lukas Miklautz, Claudia Plant, and Christian Böhm. 2023. Benchmarking deep clustering algorithms with clustpy. In *2023 IEEE International Conference on Data Mining Workshops (ICDMW)*. IEEE, 625–632.
- [18] Tao Li and Cha-charis Ding. 2018. Nonnegative matrix factorizations for clustering: A survey. *Data Clustering* (2018), 149–176.
- [19] Adam Paszke, Sam Gross, Soumith Chintala, Gregory Chanan, Edward Yang, Zachary DeVito, Zeming Lin, Alban Desmaison, Luca Antiga, and Adam Lerer. 2017. Automatic differentiation in pytorch. (2017).
- [20] F. Pedregosa, G. Varoquaux, A. Gramfort, V. Michel, B. Thirion, O. Grisel, M. Blondel, P. Prettenhofer, R. Weiss, V. Dubourg, J. Vanderplas, A. Passos, D. Cournapeau, M. Brucher, M. Perrot, and E. Duchesnay. 2011. Scikit-learn: Machine Learning in Python. *Journal of Machine Learning Research* 12 (2011), 2825–2830.
- [21] Matteo Ruffini, Ricard Gavaldà, and Esther Limon. 2017. Clustering Patients with Tensor Decomposition. In *MLHC (Proceedings of Machine Learning Research, Vol. 68)*. PMLR, 126–146.
- [22] Wei Xu, Xin Liu, and Yihong Gong. 2003. Document clustering based on non-negative matrix factorization. In *Proceedings of the 26th annual international ACM SIGIR conference on Research and development in information retrieval*. 267–273.

2611 *Data Mining, KDD '14, New York, NY, USA - August 24 - 27, 2014*. ACM, 253–262.
 2612 <https://doi.org/10.1145/262330.2623734>

2613 [10] Nam Hyeon-Woo, Moon Ye-Bin, and Tae-Hyun Oh. 2021. FedPara: Low-rank
 2614 Hadamard Product for Communication-Efficient Federated Learning. In *International
 2615 Conference on Learning Representations*.

2616 [11] George Karypis, Eui-Hong Han, and Vipin Kumar. 1999. Chameleon: Hierarchical
 2617 Clustering Using Dynamic Modeling. *Computer* 32, 8 (1999), 68–75. <https://doi.org/10.1109/2.781637>

2618 [12] Markelle Kelly, Rachel Longjohn, and Kolby Nottingham. 2023. The UCI machine
 2619 learning repository.

2620 [13] Mikhail Khodak, Neil A. Tenenholz, Lester Mackey, and Nicolò Fusi. 2021. Initializa-
 2621 tion and Regularization of Factorized Neural Layers. In *ICLR*. OpenReview.net.

2622 [14] Tamara G. Kolda and Brett W. Bader. 2009. Tensor Decompositions and Applica-
 2623 tions. *SIAM Rev* 51, 3 (2009), 455–500.

2624 [15] Yann LeCun, Léon Bottou, Yoshua Bengio, and Patrick Haffner. 1998. Gradient-
 2625 based learning applied to document recognition. *Proc. IEEE* 86, 11 (1998), 2278–
 2626 2324.

2627 [16] Daniel Lee and H Sebastian Seung. 2000. Algorithms for non-negative matrix
 2628 factorization. *Advances in neural information processing systems* 13 (2000).

2629 [17] Collin Leiber, Lukas Miklautz, Claudia Plant, and Christian Böhm. 2023. Bench-
 2630 marking deep clustering algorithms with clustpy. In *2023 IEEE International
 2631 Conference on Data Mining Workshops (ICDMW)*. IEEE, 625–632.

2632 [18] Tao Li and Cha-charis Ding. 2018. Nonnegative matrix factorizations for cluster-
 2633 ing: A survey. *Data Clustering* (2018), 149–176.

2634 [19] Adam Paszke, Sam Gross, Soumith Chintala, Gregory Chanan, Edward Yang,
 2635 Zachary DeVito, Zeming Lin, Alban Desmaison, Luca Antiga, and Adam Lerer.
 2636 2017. Automatic differentiation in pytorch. (2017).

2637 [20] F. Pedregosa, G. Varoquaux, A. Gramfort, V. Michel, B. Thirion, O. Grisel, M.
 2638 Blondel, P. Prettenhofer, R. Weiss, V. Dubourg, J. Vanderplas, A. Passos, D. Cour-
 2639 napeau, M. Brucher, M. Perrot, and E. Duchesnay. 2011. Scikit-learn: Machine
 2640 Learning in Python. *Journal of Machine Learning Research* 12 (2011), 2825–2830.

2641 [21] Matteo Ruffini, Ricard Gavaldà, and Esther Limon. 2017. Clustering Patients
 2642 with Tensor Decomposition. In *MLHC (Proceedings of Machine Learning Research,
 2643 Vol. 68)*. PMLR, 126–146.

2644 [22] Wei Xu, Xin Liu, and Yihong Gong. 2003. Document clustering based on non-
 2645 negative matrix factorization. In *Proceedings of the 26th annual international ACM
 2646 SIGIR conference on Research and development in information retrieval*. 267–273.

2647 [23] Kamal Berahmand, Mehrnoush Mohammadi, Razieh Sheikhpour, Yuefeng Li, and
 2648 Yue Xu. 2024. WSNMF: Weighted Symmetric Nonnegative Matrix Factorization
 2649 for attributed graph clustering. In *Neurocomputing*. 127041.

2650 [24] Jean-Philippe Brunet, Pablo Tamayo, Todd R Golub, and Jill P Mesirov. 2004. Meta-
 2651 genes and molecular pattern discovery using matrix factorization. In *Proceedings of
 2652 the national academy of sciences*. 4164–4169.

2653 [25] Zitai Chen, Chuan Chen, Zibin Zheng, and Yi Zhu. 2019. Tensor Decomposition
 2654 for Multilayer Networks Clustering. In *AAAI*. AAAI Press, 3371–3378.

2655 [26] Peter A. Chew, Brett W. Bader, Tamara G. Kolda, and Ahmed Abdellali. 2007. Cross-
 2656 language information retrieval using PARAFAC2. In *KDD*. ACM, 143–152.

2657 [27] Seungjin Choi. 2008. Algorithms for orthogonal nonnegative matrix factorization.
 2658 In *2008 ieee international joint conference on neural networks (ieee world congress
 2659 on computational intelligence)*. IEEE, 1828–1832.

2660 [28] Martino Ciaperoni, Aristides Gionis, and Heikki Mannila. 2024. The Hadamard
 2661 decomposition problem. *Data Mining and Knowledge Discovery* (2024), 1–42.

2662 [29] Chris Ding and Xiaofeng He. 2004. K-means clustering via principal component
 2663 analysis. In *Proceedings of the twenty-first international conference on Machine
 2664 learning*. 29.

2665 [30] Marek Gagolewski. 2022. A framework for benchmarking clustering algorithms.
 2666 *SoftwareX* 20 (2022), 101270.

2667 [31] Stephan Günnemann, Ines Färber, Matthias Sebastian Rüdiger, and Thomas Seidl.
 2668 2014. SMVC: semi-supervised multi-view clustering in subspace projections. In
 2669 *The 20th ACM SIGKDD International Conference on Knowledge Discovery and
 2670 Data Mining*. ACM, 123–131.